Advances in Geo-Energy Research

Vol. 10, No. 2, p. 91-103, 2023

Original article

Numerical well test model of oil-water two-phase flow in fractured and vuggy carbonate reservoir

Guohan Xu[1,2], Hongjun Yin[1,2]*, Daiyan Zhang[3], Jing Fu[4], Cuiqiao Xing[1,2]

[1]*Key Laboratory of Enhanced Oil Recovery (Northeast Petroleum University), Ministry of Education, Daqing 163000, P. R. China*

[2]*Department of Petroleum Engineering, Northeast Petroleum University, Daqing 163000, P. R. China*

[3]*Research Institute of Exploration and Development, Xinjiang Oilfield Company, Karamay 834000, P. R. China*

[4]*Department of Petroleum Engineering, Colorado School of Mines, Golden 80401, USA*

Keywords:
Fractured and vuggy carbonate reservoir
random natural fracture
finite volume method
oil-water two-phase flow
numerical well test

Cited as:
Xu, G., Yin, H., Zhang, D., Fu, J., Xing, C. Numerical well test model of oil-water two-phase flow in fractured and vuggy carbonate reservoir. Advances in Geo-Energy Research, 2023, 10(2): 91-103.
https://doi.org/10.46690/ager.2023.11.04

Abstract:
Fractured and vuggy carbonate reservoirs present a complex storage space with irregularly distributed fractures and caves. Furthermore, these reservoirs typically feature the presence of a substantial bottom aquifer, further complicating the fluid flow dynamics. At present, most well test models for this reservoir are based on discrete media primarily address single-phase flow scenarios, typically considering caves as equipotential bodies. This approach cannot accurately represent the complexities of such reservoirs. In this paper, a three-dimensional numerical well test model for two-phase oil-water flow within fractured and vuggy carbonate reservoirs is introduced. Randomly generated natural fractures are embedded within the reservoir, and the Hagen-Poiseuille law is utilized to describe fluid flow within cave spaces, effectively coupling flow interactions across fractures, caves and the porous rock matrix. The computational domain is discretized by a perpendicular bisection grid, and the finite volume method is used to solve the model, allowing for the calculation of the pressure and saturation fields at each time step. Subsequently, well test type curves are constructed and analyzed, flow regimes are segmented, and sensitivity analysis of model parameters is conducted. The pressure buildup data from well A are interpreted, and the results demonstrate a remarkable agreement between the well test curve and actual data, confirming the capability of the model to capture reservoir characteristics and complex fluid flow phenomena. The findings lay the foundation for the development of numerical well test models tailored to fractured and vuggy carbonate reservoirs.

1. Introduction

Fractured and vuggy carbonate reservoirs display a complex spatial morphology characterized by intricate patterns that span various length scales. These patterns encompass a highly dispersed and diverse network of connectivity, giving rise to a multitude of distinct flow configurations (Jiao, 2019; Tian et al., 2019; Huang et al., 2021). Furthermore, significant variations in both the permeability and the porosity levels can be observed within different media systems, contributing to a pronounced degree of reservoir heterogeneity (Lu et al., 2020; Zhang et al., 2023). The investigation of reservoir flow mechanisms constitutes fundamental research in the realm of oilfield development, which maintains a close and intrinsic relationship with well test studies aimed at enhancing comprehension of these complex reservoir flow mechanisms. To gain further insights into the distribution of natural fractures and cavernous structures within the reservoir, as well as to attain a comprehensive knowledge of the intricate fluid flow mechanism, it is imperative to conduct dedicated well test research that is specific to fractured and vuggy carbonate reservoirs (Jia et al., 2013; Chen et al., 2015).

Encountering caves during well drilling is the most ideal scenario (Spence, 2004; Cayeux et al., 2017). Accordingly, scholars have devoted much attention to the development of testing models tailored to this specific condition (Xing

Yandy Scientific Press

*Corresponding author.
E-mail address: xgh1219973727@163.com (G. Xu); yinhj7176@126.com (H. Yin); zhangdaiy@petrochina.com.cn (D. Zhang); jingfu@mines.edu (J. Fu); xincq888@163.com (C. Xing).

Received September 16, 2023; revised October 2, 2023; accepted October 20, 2023; available online October 24, 2023.

et al., 2018; Liu, 2022). Nonetheless, in practical drilling operations, an actual encounter with caves is not assured on every occasion. This makes it necessary to intentionally induce artificial fractures and establish connectivity with the caves through acid fracturing techniques. Fluid storage and flow are predominantly localized within the confined spaces of caves and fractures, assuming a comparatively subordinate role of the porous matrix in this context. Notably, the mobility of fluids within the cave surpasses that within other media found in fractured and vuggy carbonate reservoirs, as substantiated by prior scholarly contributions (Kang et al., 2006; Liu et al., 2019; Yang et al., 2020). Indeed, in contrast to conventional oil reservoirs, fractured and vuggy carbonate reservoirs require a comprehensive consideration of cave flow and the intricate phenomenon of interporosity flow among various geological systems (Popov et al., 2007; Liu et al., 2022). Within these reservoirs, these dynamics frequently materialize as a collective integration across diverse spatial configurations, thereby amplifying the complex and variable flow characteristics of fractured and vuggy carbonate reservoirs. These intricacies pose fresh challenges in the development of well test models (Nie et al., 2009; Guo et al., 2012).

In the context of the improving understanding of fractured and vuggy carbonate reservoirs, there is a growing need to develop well test models that can effectively account for the existence of fractures and caves. Liu et al. (2020) presented a comprehensive multi fracture-vug composite model tailored for fractured vuggy carbonate reservoirs. This model intricately divides the reservoir into distinct fracture-vug flow zones based on the distribution of caves, which can be used to conduct meticulous sensitivity analysis on its underlying parameters. In the same year, an analytical multi-zonal composite reservoir well test model with the ability to calculate vug volume was presented by Du et al. (2020). This model elucidates the reservoir characteristics by partitioning the well test curve into various flow regimes, demonstrating the existence of an additional vug in the formation results in an additional concavity in the derivative curve. Furthermore, Liu (2022) delved into the analysis of the transitory behavior of bottom hole pressure in a horizontal well producing from a confined fracture and vuggy reservoir. This approach considers the well geometry, including the skin factor, as well as the hydraulic fracturing design, which includes a number of fracture parameters.

Nevertheless, it is essential to acknowledge that the above studies make the simplifying assumption of treating caves as equipotential bodies. This assumption, while practical, oversimplifies the complex structure within caves and disregards the internal flow processes and dynamic changes within them.

In addition to the analytical well test, a numerical well test has also been used for fractured and vuggy carbonate reservoirs. Corbett et al. (2012) conducted numerical well test investigations in carbonate reservoirs characterized by three distinct pore systems. The outcomes unveiled a complex behavior, where macro-porosity demonstrated a combined response with fractures during well testing, posing challenges in differentiating the respective contributions of flow from fractures and highly permeable porous matrices. Li et al. (2017) introduced a systematic approach for the dynamic characterization of carbonate reservoirs, emphasizing the analysis of production data and well test findings. This was applied to the fractured-caved carbonate reservoir, where diverse numerical reservoir models were constructed and well test-type curves were generated to facilitate the evaluation of reservoir types. Furthermore, Sun et al. (2023) established a numerical well test model tailored for fractured reservoirs, which thoughtfully accounted for both the matrix system and the fracture system, including large faults and small fractures. This model integrates randomly generated natural fracture networks with unstructured discrete fracture modeling, effectively elucidating the disparities in well productivity and the notably swift inter-well pressure response. In comparison to their analytical counterparts, numerical well test methods furnish a more comprehensive depiction of the intricate interplay among the pore system, fracture system and cave system within fractured and vuggy carbonate reservoirs. Consequently, they offer a more precise portrayal of fluid flow within the reservoir and provide greater flexibility in incorporating fractures and caves into the modeling framework. When the pores within a cave are relatively large and exhibit good connectivity, the flow inside the cave can be considered laminar flow. Furthermore, the laminar flow of incompressible viscous fluids in narrow conduits can be equivalent to Hagen-Poiseuille flow (Xie et al., 2018; Lin et al., 2021). Therefore, the fluid flow within the cave can be approximated as Hagen-Poiseuille flow, enabling the coupling of flow between different media.

Existing well test models primarily focus on single-phase flow conditions, thus may not accurately represent the behavior of fractured and vuggy carbonate reservoirs, which often include a bottom aquifer (Li and Wang, 2016; Tang et al., 2023). Neglecting two-phase oil-water flow can result in interpretation errors. Kolin et al. (2018) effectively utilized Eclipse software for simulating pressure transient tests involving two-phase flow in a homogeneous reservoir. This approach provided valuable insights into the absolute permeability of the reservoir and the skin factor of the production well, with applicability to real reservoir systems featuring multiphase fluid flow within porous media. Kamal et al. (2019) introduced an innovative method that leverages transient well testing to accurately estimate the $in-situ$ absolute permeability of reservoir formations, even under the simultaneous flow of three fluid phases. The validity of this method was established through simulations using synthetic data. Wang et al. (2023) established a model for analyzing oil-water two-phase flow pressure transient data in polymer flooding fractured wells. The study involved sensitivity analysis of the model parameters and demonstrated the reliability and practicality of the proposed model. Although significant progress has been made in the numerical simulation of two-phase flow, a notable gap remains in the development of analysis methods tailored specifically to two-phase flow well tests in fractured and vuggy carbonate reservoirs with a bottom aquifer.

The current study presents a comprehensive approach to address the complexities of oil-water two-phase flow in fractured and vuggy carbonate reservoirs, particularly those with a bottom aquifer. The methodology involves introducing

randomly generated natural fractures into the reservoir and employing the Hagen-Poiseuille equation to model flow within these caves. This integrated approach allows for the coupling of flow between caves, fractures and the porous rock matrix, resulting in the development of a robust three-dimensional numerical well test model. The finite volume method is applied to solve this model, enabling the calculation of pressure and saturation fields at different time intervals. Furthermore, well test type curves are constructed, facilitating the categorization of flow regimes, and sensitivity analyses of the model parameters are performed. The findings of this research contribute not only to the theoretical understanding of numerical well test methods for fractured and vuggy carbonate reservoirs but also provide insights into practical aspects for potential applications in the industry.

2. Methods

2.1 Random generation of natural fractures

The distribution of natural fractures is of paramount importance in establishing a sound physical model for the reservoir, which utilizes a methodology employing random point selection, random azimuth assignment, random length determination, and random width allocation (Sun and Schechter, 2015; Dong et al., 2021). The selection of random point $P(x)$ is accomplished through the application of a discrete random number generation technique. This method offers the flexibility to tailor the distribution of random numbers in accordance with specific criteria, enabling adjustments to the distribution and density of the fractures to align with the desired geological characteristics.

The following constraints are imperative when generating random natural fractures:

1) Fracture azimuth angle: To account for the impact of regional crustal stress, all natural fractures within the model are subject to a constraint on their azimuth angles. These angles are confined to a reasonable interval and demonstrate a specific degree of convergence. In this study, the azimuth angles of the constrained natural fractures are limited to the range between north and east directions.
2) Fracture length: Drawing upon insights from field fracture surveys and recognizing that the dimensions of micro-fractures within natural fractures are typically limited, this study imposes constraints on the length of these fractures. Specifically, the length of micro-fractures is constrained to be < 30 meters, and the width is restricted to be < 1 meter.
3) Distribution density: The distribution density of natural fractures is derived from field data conducted in fractured and vuggy carbonate reservoirs. Statistical processing of this distribution density data is undertaken to establish the probability density function governing the distribution of natural fractures within the study area:

$$f(x,y)=\begin{cases}\frac{1}{LW} & 0<x<L, 0<y<W\\ 0 & x\le 0, y\le 0, x\ge L, y\ge W\end{cases} \tag{1}$$

The mathematical description for generating random fractures is based on random numbers that adhere to a uniform distribution, as presented below:

$$P_x = LR_x, P_y = WR_y \tag{2}$$

$$\theta_P = \frac{\pi}{2}R_\theta,\ l_P = l_{\max}R_l,\ w_P = w_{\max}R_w,\ F_{cP} = F_{c\max}R_{F_c} \tag{3}$$

where L and W are reservoir length and width respectively, m; R_a is a generated random number in the range a; subscripts $a = x, y, \theta, l, w$ and F_c, represent x-coordinate, y-coordinate, azimuth angle range, length range, width range and fracture conductivity range respectively. P_x and P_y are the horizontal and vertical coordinates of random points respectively; θ_P is the fracture azimuth angle, rad; l_P and w_P are the length and width of the fracture, m; F_{cP} is fracture conductivity, mD·m; $l_{\max}$ and $w_{\max}$ are the maximum reasonable length and width of random natural fractures respectively, m; $F_{c\max}$ is the maximum reasonable fracture conductivity, mD·m; R_a is a generated random number in the range a; subscripts a = θ, l, w and F_c, represent azimuth angle range, length range, width range and fracture conductivity range, respectively.

By acknowledging the multiscale nature of natural fractures, it becomes feasible to superimpose two distinct categories of fractures within the reservoir, distinguishing between large-scale fractures and micro-fractures. This strategy enables the assignment of distinct parameters for each fracture category, encompassing characteristics such as fracture length and conductivity. As a result, this method facilitates the representation of multiscale fractures within fractured and vuggy carbonate reservoirs, as depicted in Fig. 1. In light of the aforementioned adjustments, random fractures are generated multiple times, and one of these realizations is selected to align with field fracture distribution data to ultimately establish the physical model.

2.2 Establishment of physical model

Multiple assumptions are made about the physical model, including: (1) The presence of oil-water two-phase porous media flow in the reservoir; (2) the compressibility of both rocks and fluids in the reservoir; (3) adherence to Darcy's law for fluid flow in the reservoir through porous rock matrix and fractures; (4) compliance with the Hagen-Poiseuille law for fluid flow inside the cave; (5) consideration of the influence of gravity and capillary pressure; and (6) the existence of a bottom aquifer in the reservoir.

In fractured and vuggy carbonate reservoirs, pores are uniformly distributed within the porous rock matrix, and natural fractures (including micro-fractures and large-scale fractures) as well as caves are randomly generated in the reservoir. Wells may or may not encounter caves during drilling. Fig. 2 illustrates the scenario in which a well does not encounter caves. On the left side of the well, the brown area in the figure represents caves and the well is connected to the caves through

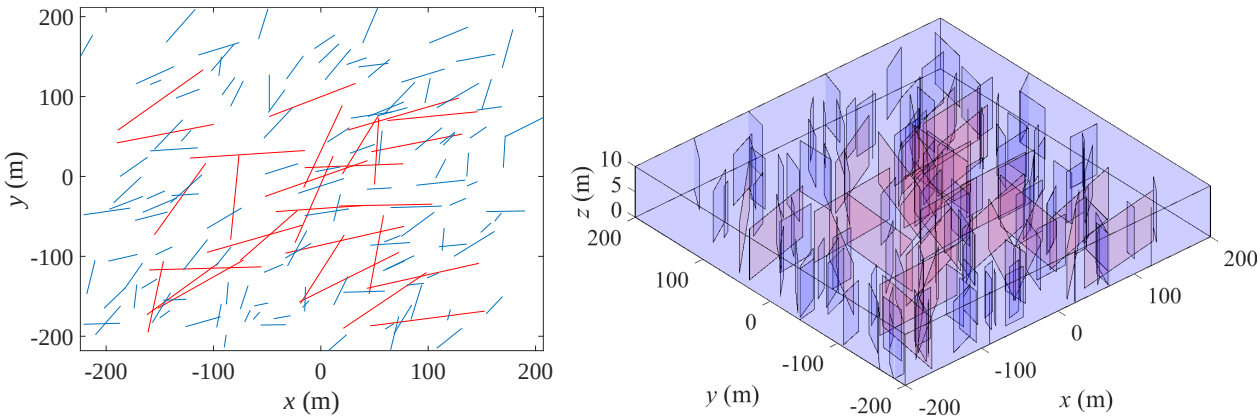

(a) Two-dimensional diagram (b) Three-dimensional diagram

Fig. 1. Randomly generated multi-scale natural fracture distribution map.

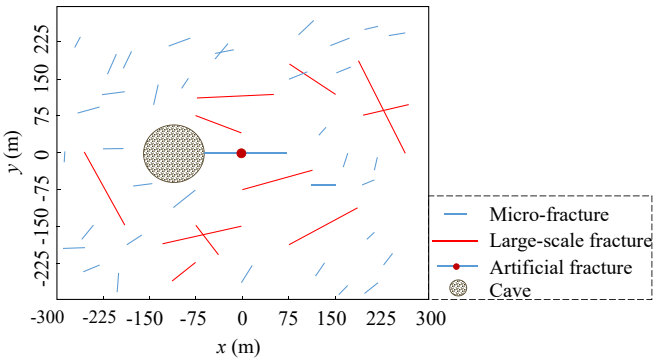

Fig. 2. Physical model of the fractured and vuggy carbonate reservoir.

Table 1. Natural fracture parameters.

Parameter	Value range
Large-scale fracture number	11
Large-scale fracture length, m	30-200
Large-scale fracture width, m	0.4-1.2
Large-scale fracture permeability, mD	1,500-3,000
Large-scale fracture conductivity, mD·m	600-3,600
Micro-fracture number	36
Micro-fracture length, m	10-30
Micro-fracture width, m	0.1-1
Micro-fracture azimuth angle, rad	0-π/2
Micro-fracture permeability, mD	1,000-2,500
Micro-fracture conductivity, mD·m	100-2,500

artificial fractures. Table 1 lists the parameters of random natural fractures.

Considering natural fractures, caves and various well types in the fractured and vuggy carbonate reservoir, the computational area is divided using a three-dimensional perpendicular bisection grid, as depicted in Fig. 3.

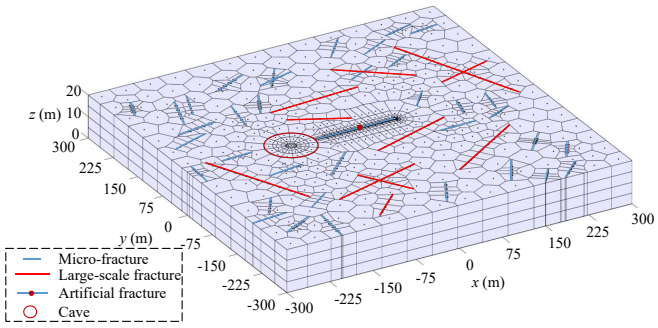

Fig. 3. The result of mesh generation.

2.3 Establishment of mathematical model

Based on the law of mass conservation, the continuity equations for transient flow in porous media for both the oil and water phases, which include source terms, can be expressed as follows:

$$-\nabla(\rho_o v_{o\alpha}) + \rho_o \hat{q}_o = \frac{\partial(\phi_\alpha \rho_o S_o)}{\partial t} \tag{4}$$

$$-\nabla(\rho_w v_{w\alpha}) + \rho_w \hat{q}_w = \frac{\partial(\phi_\alpha \rho_w S_w)}{\partial t} \tag{5}$$

where ρ_o and ρ_w are the oil and water density respectively, kg/m^3; v_o and v_w are the oil and water flow velocity respectively, m/s; S_o and S_w are the oil and water saturation, respectively, $S_o + S_w = 1$; t is the time, s; $\hat{q}_o$ and $\hat{q}_w$ are the oil and water unit volume flow rate respectively, 1/s; ϕ_α is the reservoir porosity; subscript $\alpha = m$, f and v represent matrix system, fracture system and cave system respectively.

For the matrix system and the fracture system, considering the gravity and capillary pressure, the two-phase flow equations based on Darcy's law are given as:

$$v_{o\beta} = -\frac{k_\beta k_{ro\beta}}{\mu_o}\left(\nabla p_{o\beta} + \rho_o g \nabla D\right) \tag{6}$$

$$v_{w\beta} = -\frac{k_\beta k_{rw\beta}}{\mu_w}\left(\nabla p_{o\beta} - \nabla p_{c\beta} + \rho_w g \nabla D\right) \tag{7}$$

where k_β is the permeability, m^2, subscript $\beta = m$ and f

represents matrix system and fracture system respectively; k_{ro} and k_{rw} are the relative permeability of oil and water phase respectively; μ_o and μ_w are the oil and water viscosity respectively, Pa·s; $p_{o\beta}$ and $p_{w\beta}$ are oil and water pressure respectively, Pa; g is gravitational acceleration, m/s^2; D is reservoir depth, m; $p_{c\beta}$ is capillary pressure, $p_{c\beta}=p_{o\beta}-p_{w\beta}$, Pa.

For the cave system, assuming the laminar flow of liquid inside the cave, it can be described using the modified Hagen-Poiseuille law that takes gravity into account:

$$v_{ov}=-\frac{\rho_o A_o}{8\pi\mu_o}\left(\nabla p_{ov}+\rho_o g\nabla D\right) \tag{8}$$

$$v_{wv}=-\frac{\rho_w A_w}{8\pi\mu_w}\left(\nabla p_{wv}+\rho_w g\nabla D\right) \tag{9}$$

where A_o and A_w are the flow area of oil phase and water phase respectively, $A_o=AS_o$, $A_w=AS_w$, m^2; A is the flow area, m^2; p_{ov} and p_{wv} are oil and water pressure in the cave system respectively, Pa; subscript v represents the cave system.

By substituting Eqs. (6)-(7) into the Eqs. (4)-(5), the basic differential equations in the matrix system and the fracture system are obtained as follows:

$$\begin{aligned}&\nabla\cdot\left[\frac{\rho_o k_\beta k_{ro\beta}}{\mu_o}\left(\nabla p_{o\beta}+\rho_o g\nabla D\right)\right]+\rho_o\hat{q}_o\\&=\rho_o S_o\phi_\beta\left(c_\phi+c_o\right)\frac{\partial p_o}{\partial t}+\phi_\beta\rho_o\frac{\partial S_o}{\partial t}\end{aligned} \tag{10}$$

$$\begin{aligned}&\nabla\cdot\left[\frac{\rho_w k_\beta k_{rw\beta}}{\mu_w}\left(\nabla p_{o\beta}-\nabla p_{c\beta}+\rho_w g\nabla D\right)\right]+\rho_w\hat{q}_w\\&=\rho_w S_w\phi_\beta\left(c_\phi+c_w\right)\frac{\partial p_w}{\partial t}+\phi_\beta\rho_w\frac{\partial S_w}{\partial t}\end{aligned} \tag{11}$$

Similarly, the basic differential equations in cave system are obtained as follows:

$$\begin{aligned}&\nabla\left[\frac{\rho_o A_o}{8\pi\mu_o}\left(\nabla p_{ov}+\rho_o g\nabla D\right)\right]+\rho_o\hat{q}_o\\&=\rho_o S_o\phi_v\left(c_v+c_o\right)\frac{\partial p_o}{\partial t}+\phi_v\rho_o\frac{\partial S_o}{\partial t}\end{aligned} \tag{12}$$

$$\begin{aligned}&\nabla\left[\frac{\rho_w A_w}{8\pi\mu_w}\left(\nabla p_w+\rho_w g\nabla D\right)\right]+\rho_w\hat{q}_w\\&=\rho_w S_w\phi_v\left(c_v+c_w\right)\frac{\partial p_w}{\partial t}+\phi_v\rho_w\frac{\partial S_w}{\partial t}\end{aligned} \tag{13}$$

where c_ϕ, c_o and c_w are the rock compressibility, oil compressibility and water compressibility respectively, Pa^{-1}.

2.4 Solution of mathematical model

The basic differential equations of the matrix system and fracture system are established, which are obtained by adding Eq. (10) to Eq. (11) :

$$\begin{aligned}&\nabla\cdot\left[k_\beta\left(\lambda_t\nabla p_{o\beta}+\left(\lambda_w\gamma_w+\lambda_o\gamma_o\right)\nabla D-\lambda_w\nabla p_{c\beta}\right)\right]+\hat{q}_t\\&=\phi_\beta c_t\frac{\partial p_{o\beta}}{\partial t}\end{aligned} \tag{14}$$

where c_t is the total compressibility, Pa^{-1}.

$$\lambda_o=k_{r\beta}/\mu_o,\quad \lambda_w=k_{rw\beta}/\mu_w \tag{15}$$

$$\gamma_o=\rho_o g,\quad \gamma_w=\rho_w g \tag{16}$$

$$c_t=c_\phi+S_o c_o+S_w c_w \tag{17}$$

$$\hat{q}_t=\hat{q}_o+\hat{q}_w\quad \lambda_t=\lambda_o+\lambda_w \tag{18}$$

A volume integral is performed on Eqs. (11) and (14):

$$\begin{aligned}&\iiint_{V_i}\nabla\cdot\left[k_\beta\left(\lambda_t\nabla p_{o\beta}+\left(\lambda_w\gamma_w+\lambda_o\gamma_o\right)\nabla D-\lambda_w\nabla p_{c\beta}\right)\right]\mathrm{d}\Omega\\&+\iiint_{V_i}\hat{q}_t\mathrm{d}\Omega=\iiint_{V_i}\phi_\beta c_t\frac{\partial p_{o\beta}}{\partial t}\mathrm{d}\Omega\end{aligned} \tag{19}$$

$$\begin{aligned}&\iiint_{V_i}\left[\nabla\cdot k_\beta\lambda_w\left(\nabla p_{w\beta}-\nabla p_{c\beta}+\gamma_w\nabla D\right)\right]\mathrm{d}\Omega+\iiint_{V_i}\hat{q}_w\mathrm{d}\Omega\\&=\iiint_{V_i}\left[S_w\phi\left(c_\phi+c_w\right)\frac{\partial p_{w\beta}}{\partial t}+\phi_\beta\frac{\partial S_w}{\partial t}\right]\mathrm{d}\Omega\end{aligned} \tag{20}$$

where V_i is the volume of grid i, m^3.

Using Gauss's theorem, the implicit format of Eqs. (19)-(20) is obtained as follows:

$$\begin{aligned}&\sum_j\left(T_{ij,t}\Delta p_{o\beta}\right)^{n+1}+\sum_j\left[\left(T_{ij,o}\gamma_o+T_{ij,w}\gamma_w\right)\Delta D\right]^n\\&-\sum_j\left(T_{ij,w}\Delta p_{c\beta}\right)^n+q_t^{n+1}=\frac{V_i\phi c_t}{\Delta t}\left(p_{o\beta}^{n+1}-p_{o\beta}^n\right)\end{aligned} \tag{21}$$

$$\begin{aligned}&\sum_j\left(T_{ij,w}\Delta p_{w\beta}\right)^{n+1}+\sum_j\left(T_{ij,w}\gamma_w\Delta D\right)^n-\sum_j\left(T_{ij,w}\Delta p_{c\beta}\right)^n+q_w^{n+1}\\&=\frac{V_i\phi_\beta S_w^n\left(c_\phi+c_w\right)}{\Delta t}\left(p_{w\beta}^{n+1}-p_{w\beta}^n\right)+\frac{V_i\phi_\beta}{\Delta t}\left(S_w^{n+1}-S_w^n\right)\end{aligned} \tag{22}$$

The conduction coefficient is defined as follows:

$$T_{ij,l}=\left(\frac{k_\beta k_{rl\beta}}{\mu_l}\right)_{ij}\frac{\omega_{ij}}{d_{ij}} \tag{23}$$

where T_{ij} is the conduction coefficient between grid i and grid j, m^3/(Pa·s); ω_{ij} is the contact area between grid i and grid j, m^2; d_{ij} is the distance between grid i and grid j, m; and the subscript $l=o$, w indicates the oil phase and water phase, respectively.

As for the cave system, Eqs. (24)-(25) are obtained:

$$\begin{aligned}&\sum_j\left(T_{vij,t}\Delta p_{ov}\right)^{n+1}+\sum_j\left[\left(T_{vij,o}\gamma_o+T_{vij,w}\gamma_w\right)\Delta D\right]^n+q_t^{n+1}\\&=\frac{V_i\varphi_v c_{tv}}{\Delta t}\left(p_{ov}^{n+1}-p_{ov}^n\right)\end{aligned} \tag{24}$$

$$\begin{aligned}&\sum_j\left(T_{vij,w}\Delta p_{wv}\right)^{n+1}+\sum_j\left(T_{vij,w}\gamma_w\Delta D\right)^n+q_w^{n+1}\\&=\frac{V_i\phi_v S_w^n\left(c_v+c_w\right)}{\Delta t}\left(p_{wv}^{n+1}-p_{wv}^n\right)+\frac{V_i\phi_v}{\Delta t}\left(S_w^{n+1}-S_w^n\right)\end{aligned} \tag{25}$$

where T_{vij} is the conductivity coefficient of the cave system, m^3/(Pa·s).

$$T_{vij,l}=\frac{A_{ij,l}}{8\pi}\left(\frac{1}{\mu_l}\right)_{ij}\frac{\omega_{ij}}{d_{ij}} \tag{26}$$

The description of cave interporosity flow is presented as follows. The grids within the red line area are considered con-

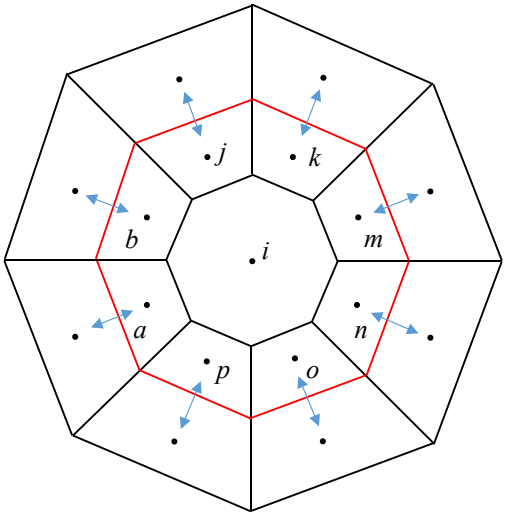

Fig. 4. Schematic diagram of cave interporosity flow.

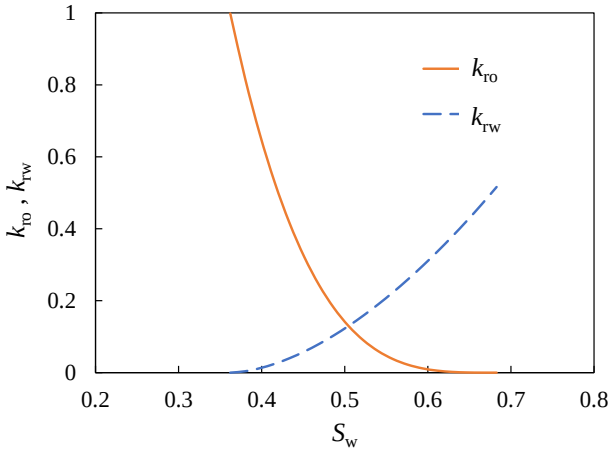

Fig. 5. Relative permeability curve.

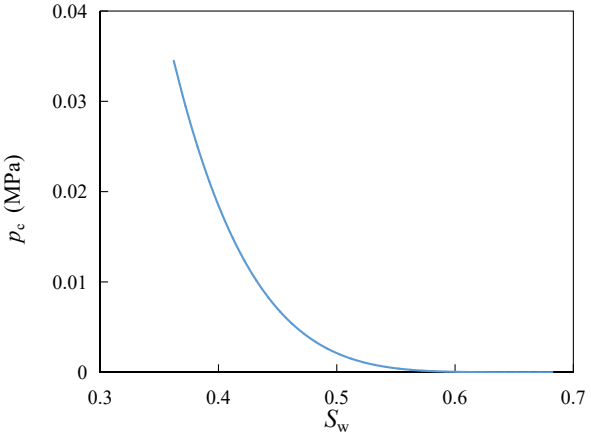

Fig. 6. Capillary pressure curve.

stituents of the cave grid, as illustrated in Fig. 4. The interior section of the cave is characterized by Hagen-Poiseuille flow, while the external section is governed by Darcy flow. At the interface between these two regions, interporosity flow occurs due to the pressure gradient.

The initial conditions of reservoir pressure and water saturation can be represented as:

$$p_m|_{t=0} = p_f\big|_{t=0} = p_v|_{t=0} = p_i \tag{27}$$

$$S_w|_{t=0} = S_{wi} \tag{28}$$

where p_i is the initial reservoir pressure, Pa; S_{wi} is the initial reservoir water saturation.

Consider the external boundary closed, indicating no flow on the boundary:

$$T_{ij,l}[p_j - p_i] = 0 \tag{29}$$

The well grid is adjacent to multiple grids, and the flow rate from the surrounding grids towards the bottom of the well is:

$$q_l = \frac{2\pi k k_{rl} h\left(p_l - p_{wf}\right)}{B_l \mu_l \left[\ln\left(r_e/r_w\right) + S\right]} = J_l\left(p_l - p_{wf}\right) \tag{30}$$

where q_l is the well production rate, m^3/d; p_{wf} is wellbore pressure, Pa; r_e is the equivalent radius, m; r_w is the wellbore radius, m; B_l is the formation volume factor; S is the skin; J_l is the production index of the well, $m^3/(Pa{\cdot}s)$.

If the constant production rate of the well is a stable value, the total production rate q_t from the formation will be:

$$q_t = \sum_j \left(J_o + J_w\right)\left(p_j - p_{wf}\right) \tag{31}$$

where p_j is the pressure of grid j, which connected to the well grid, Pa.

When considering the wellbore storage coefficient, the total production rate q_t is given by:

$$q_t^{n+1} = \sum_j \left(J_o + J_w\right)\left(p_j - p_{wf}\right) - \frac{C}{\Delta t}\left(p_{wf}^{n+1} - p_{wf}^{n}\right) \tag{32}$$

where C is wellbore storage coefficient, m^3/Pa.

3. Results and discussion

3.1 Well test type curve

The basic reservoir and fluid parameters are shown in Table 2.

When there is no special explanation, the vertical permeability is one-tenth of the horizontal permeability.

By utilizing the fundamental parameters outlined in Tables 1 and 2 and incorporating the relative permeability curve in Fig. 5 and capillary pressure curve in Fig. 6 for modeling, the wellbore pressure and its pressure derivative at each specific time point are computed. Subsequently, a well test type curve is generated, which is visually represented in Fig. 7. Upon examining the figure, it becomes evident that there exist seven distinct regimes governing fluid flow within fractured and vuggy carbonate reservoirs.

1) Pure wellbore storage regime: This regime is primarily influenced by wellbore storage. In logarithmic coordinates, the pressure difference curve aligns with the pressure derivative curve, both exhibiting a unit slope.
2) Transition flow regime: After the wellbore storage effect has subsided, the pressure difference curve and pressure

Table 2. Basic parameters.

Parameter	Value	Parameter	Value
Matrix porosity	0.25	Initial water saturation	0.4
Fracture porosity	0.02	Oil phase formation volume factor	1.1
Reservoir thickness, m	20	Water phase formation volume factor	1.0
Initial pressure, MPa	52.59	Wellbore storage coefficient, m^3/MPa	0.02
Matrix permeability, mD	1.0	Skin	-0.5
Viscosity of oil phase, mPa·s	6.5	Cave volume, m^3	9,000
Viscosity of water phase, mPa·s	1.0	Cave porosity	0.4
Rock compressibility, MPa^{-1}	4.35×10^{-4}	Cave compressibility, MPa^{-1}	5.5×10^{-4}
Oil phase compressibility, MPa^{-1}	9.24×10^{-4}	Well Radius, m	0.0878
Water phase compressibility, MPa^{-1}	5.8×10^{-4}	Artificial fracture width, m	0.05
Oil phase density, kg/m^3	790	Artificial fracture half-length, m	40
Water phase density, kg/m^3	1,000	Artificial fracture conductivity, mD·m	1,524
Reservoir depth, m	7,640	Liquid rate of production well, m^3/d	50

derivative curve gradually deviate from a straight line with a unit slope, evolving into curved trajectories.

3) Bilinear flow regime: Within this regime, the fluid exhibits linear flow along the artificial fracture and perpendicular to the fracture in the reservoir. The slope of the pressure derivative curve in this scenario is 1/4.
4) Formation linear flow regime: After the bilinear flow regime, the fluid within the reservoir flows linearly into fractures. In this flow regime, the slope of the pressure derivative curve is 1/2.
5) Cave interporosity flow and natural fracture effect regime: This regime encompasses the combined influence of caves and natural fractures. As pressure propagates to the location of a cave, fluid mobility in the karst cave media surpasses that of other media, leading to a rapid pressure drop inside the cave and interporosity flow with the surrounding medium until equilibrium is achieved. Additionally, natural fractures are distributed throughout the reservoir that display better mobility than the matrix. Consequently, the pressure derivative curve exhibits a characteristic "dip".
6) Pseudo-radial flow regime: In cases where boundaries are extensive, fluid flow in the formation approximates radial flow before the pressure wave reaches the boundaries. Under logarithmic coordinates, the pressure derivative curve approaches a nearly horizontal straight line.
7) Pseudo-steady flow regime: As pressure reaches a boundary and enters a pseudo-steady flow regime, the pressure difference curve and the pressure derivative curve both exhibit an upward trend with a unit slope.

3.2 Parameter sensitivity analysis

Using the fundamental parameters from Tables 1 and 2, the wellbore pressure data can be computed for different parameter values, providing insight into the influence of model parameters on the well test curves when plotted in log-log coordinates.

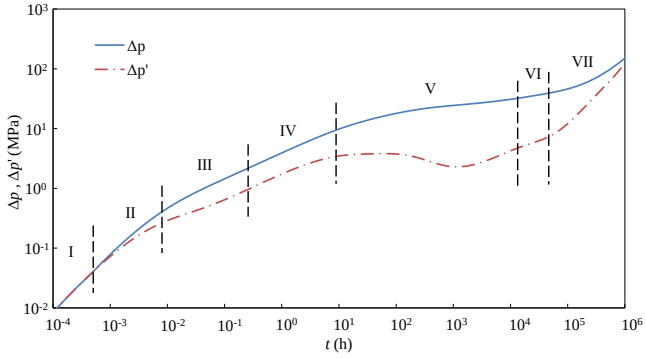

Fig. 7. Well test type curves.

(1) Effect of production time

As production time progresses, the pressure field at different times can be examined as shown in Fig. 8. Initially, pressure is rapidly transmitted through the artificial fractures and caves, resulting in a significant pressure decrease along the direction of the artificial fractures. With the extension of simulation time, pressure spreads outward from the central point of the well, leading to a gradual reduction in formation pressure. The pressure gradients prompt interporosity flow between the caves and the surrounding media. Due to the higher mobility of the water phase in the reservoir compared to the oil phase, water saturation near the wellbore increases during the oil well production process. The presence of caves, natural fractures and a bottom aquifer, along with low flow resistance in the cave and fracture systems, contributes to a complex flow pattern, resulting in uneven pressure and oil saturation distribution.

(2) Effect of bottom aquifer zone

While keeping all other parameters constant, the well test curves under two scenarios are examined: one with a bottom aquifer zone and the other without it. From Fig. 9, it is evident

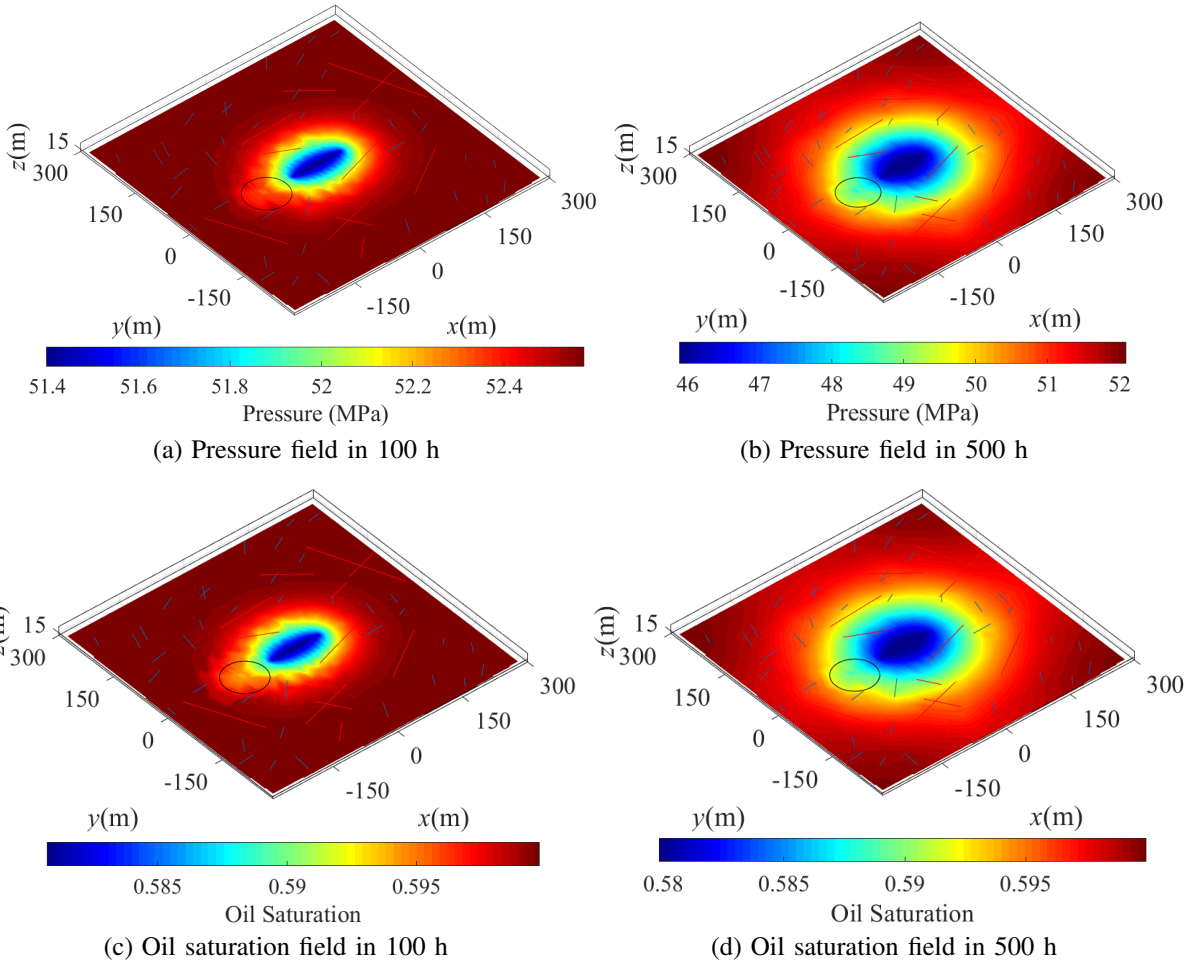

(a) Pressure field in 100 h

(b) Pressure field in 500 h

(c) Oil saturation field in 100 h

(d) Oil saturation field in 500 h

Fig. 8. Pressure field and oil saturation field during simulation.

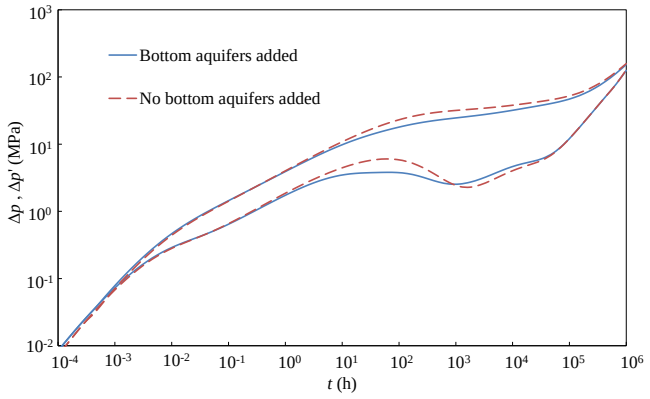

Fig. 9. Influence of bottom aquifer zone on the well test type curves.

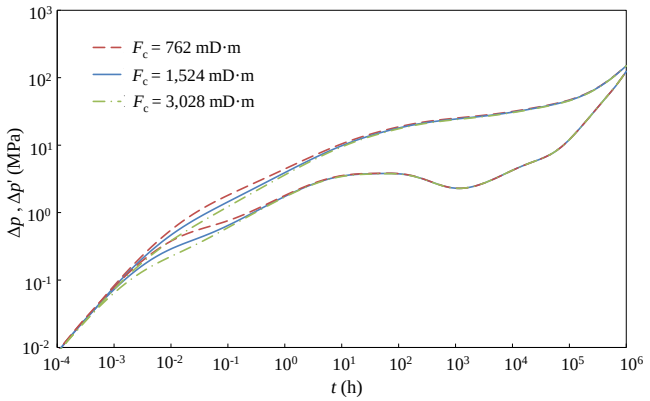

Fig. 10. Influence of artificial fracture conductivity on the well test type curves.

that the presence of a bottom aquifer zone significantly diminishes the pressure curve during the interporosity flow regime. This is due to the fact that a reservoir with a bottom water layer receives an energy supplement, subsequently reducing the flow resistance during the pressure transmission process. Moreover, the bottom aquifer zone contributes to a smoother pressure derivative curve during the interporosity flow regime compared to the scenario without it.

(3) Effect of artificial fracture conductivity

While keeping all other parameters constant, the impact of varying the artificial fracture conductivity F_c on the well test curve is analyzed. As seen in Fig. 10, artificial fracture conductivity predominantly influences the fracture linear flow regime. As the fracture conductivity increases (F_c = 762 mD·m, 1,524 mD·m, 3,048 mD·m), the bilinear flow phase concludes earlier, and the characteristics of reservoir linear fl-

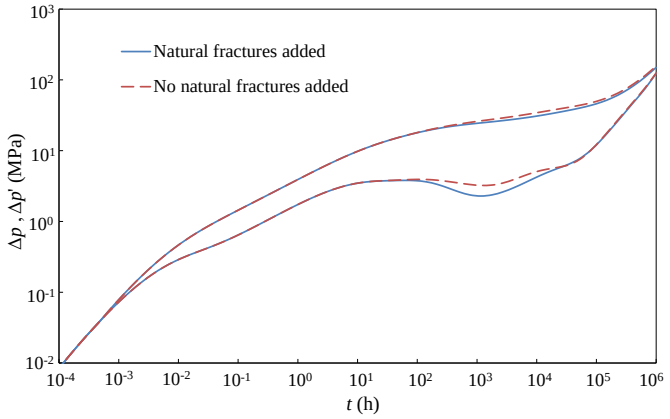

Fig. 11. Influence of natural fractures on the well test type curves.

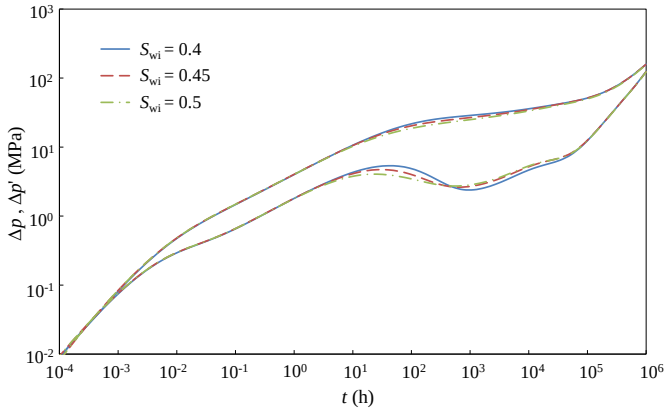

Fig. 12. Influence of initial water saturation on the well test type curves.

ow become more pronounced.

(4) Effect of natural fractures

While keeping all other parameters constant, the well test curves are explored under two scenarios: one without natural fractures and the other with natural fractures within the reservoir, as displayed in Fig. 11. The influence of natural fractures is the most prominent in the natural fracture effect regime of the well test curve. The presence of these fractures leads to a noticeable drop in the curve during this regime. This can be ascribed to the superior mobility of natural fractures compared to the matrix, reducing resistance to fluid flow and consequently causing declines in both the pressure curve and the pressure derivative curve.

(5) Effect of initial water saturation

While keeping all other parameters constant, the impact of varying the initial water saturation S_{wi} on the well test curve is investigated, as demonstrated in Fig. 12. The graph illustrates that as the initial water saturation of the oil reservoir increases (S_{wi} = 0.4, 0.45, 0.5), the pressure curve during the interporosity flow regime experiences a decrease and contributes to a smoother pressure derivative curve.

(6) Effect of cave volume

While keeping all other parameters constant and controlling the cave center position, the effect of varying the volume

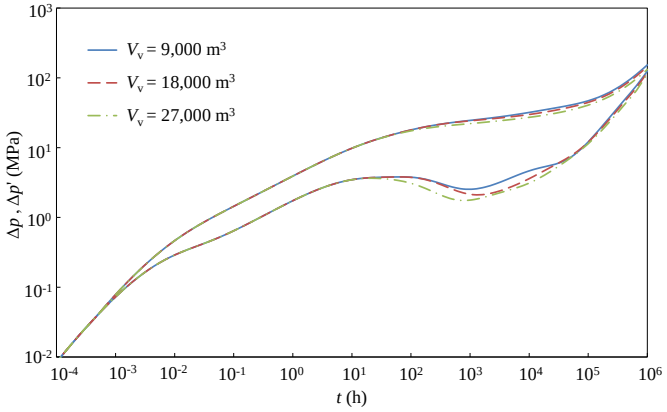

Fig. 13. Influence of cave volume on well test type curves.

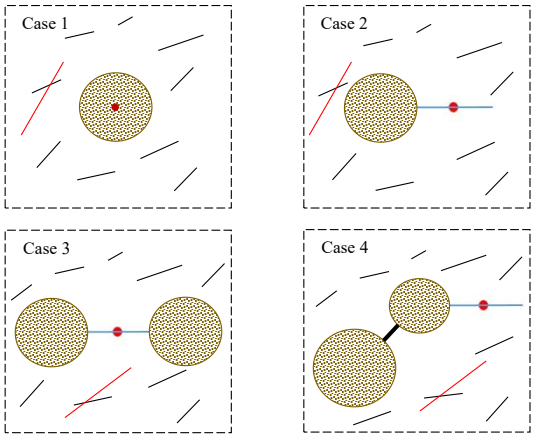

Fig. 14. Influence of cave volume on well test type curves.

of the cave V_v on the well test curve is examined, as presented in Fig. 13. In this context, the cave volume primarily affects the cave interporosity flow regime of the well test curve, leading to a pronounced dip in the curve due to the presence of the cave. When the cave volume increases (V_v = 3,500 m^3, 25,800 m^3, 36,000 m^3), the energy storage coefficient also rises. This leads to a longer duration of the cave interporosity flow regime and a greater depth of the pressure derivative curve.

(7) Effect of number and location of caves

When all other parameters are kept constant, four distinct scenarios are created by altering the quantity and placement of caves, as portrayed in Fig. 14. The four cases are as follows: Encountering a cave during well drilling; one cave located below and to the left of the well; two caves symmetrically located with respect to the well; and two caves (one large and one small) both located below and to the left of the well and connected by fractures. The effect of these scenarios on the well test curve is displayed in Fig. 15.

In Fig. 15, a comprehensive analysis of four distinct cases sheds light on the impact of caves on well test curves within fractured and vuggy carbonate reservoirs. In the context of comparing Case 1 and Case 2, the temporal influence of cave-related effects is notably accelerated when a cave is encountered during well drilling. In contrast to scenarios where cave encounters are absent, this acceleration is evident in the earlier and more substantial manifestation of a ”dip” in the

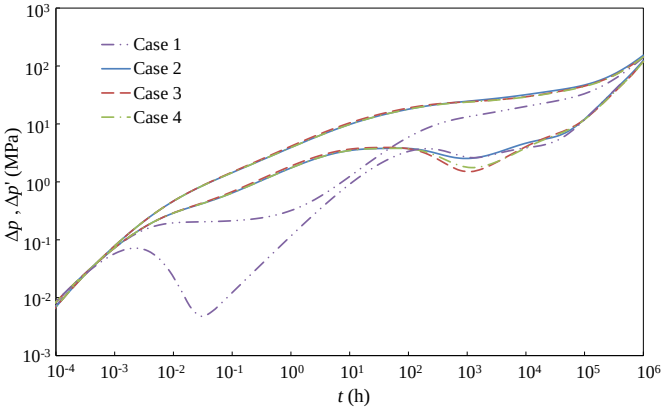

Fig. 15. Influence of number and location of caves on the well test type curves.

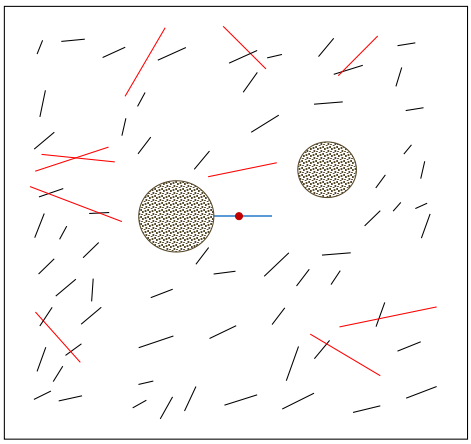

Fig. 16. Physical model of well A in fractured and vuggy carbonate reservoir.

well test curve. In situations devoid of cave encounters, which pertain to Cases 2, 3 and 4, the number and spatial arrangement of caves predominantly dictate the post-cave interporosity flow regime behavior of the well test curve. When scrutinizing the contrast between Case 2, Case 3 and Case 4, it becomes apparent that an increased number of caves or narrowing the distance between the cave and the well (Case 3) results in a more pronounced decline in the curve.

3.3 Field example

Well A is a production well situated within a fractured carbonate reservoir, featuring open hole completion and acid fracturing. The primary target layer is Ordovician limestone, and a comprehensive lithology analysis confirms the existence of pores, caves and natural fractures. An examination of measured data from the exploration well reveals instances of drill pipe venting and drilling fluid leakage during the drilling process. These occurrences suggest the presence of caves or fractures that communicate with the cave system within the reservoir. Besides, there is a significant volume of water located at the bottom of the wellbore in this well, and fractures play a vital role in connecting these subsurface features. The

Table 3. Parameters of natural fractures.

Parameter	Value
Number of large-scale fractures	10
Number of micro-fractures	64
Large-scale fracture length, m	50-300
Large-scale fracture width, m	0.2-1.2
Large-scale fracture permeability, mD	1,000-3,000
Large-scale fracture conductivity, mD·m	200-3,600
Micro-fracture length, m	10-40
Micro-fracture width, m	0.1-0.8
Micro-fracture azimuth angle, rad	0-π/2
Micro-fracture permeability, mD	500-2,500
Micro-fracture conductivity, mD·m	50-2,000

drilling depth of the well extends to 5,730.0 m, and it boasts a wellbore radius of 0.075 m. Furthermore, the reservoir exhibits a porosity of 0.2. The effective reservoir thickness is 19.5 m, the oil phase density is 0.834 g/cm^3, the water phase density is 1 g/cm^3, the oil phase viscosity is 6.46 mPa·s, and the water phase viscosity is 1.0 mPa·s. The oil phase formation volume factor is 1.1 m^3/m^3, and the water phase formation volume factor is 1 m^3/m^3. The rock compressibility is 4.35×10^{-4} MPa^{-1}, the oil compressibility is 9.24×10^{-4} MPa^{-1}, and the water compressibility is 5.80×10^{-4} MPa^{-1}.

Prior to the pressure buildup test, well A underwent production at a cumulative rate of 180.0 m^3/D while maintaining an average water cut of 31% over a total duration of 807.7 hours. Subsequently, the well was temporarily shut down for a period of 260.74 hours to facilitate the execution of a pressure buildup test. The numerical well test model established in this paper was employed to simulate the test. The physical model utilized in this simulation is illustrated in Fig. 16. The detailed parameters pertaining to the natural fractures utilized in this model can be found in Table 3.

The wellbore pressure and pressure derivative for well A are calculated at various time intervals and then the simulated theoretical curve is compared to the actual well test curve. The interpretation results are presented in Table 4, while the matching curves in a log-log plot and the pressure history matching plot are illustrated in Fig. 17. The log-log plot and the pressure history matching plot reveals a strong alignment between the data points and the curve. This alignment substantiates the suitability of the model proposed in this article for fractured and vuggy carbonate reservoirs.

The pressure field plot and saturation field plot at the end of the pressure buildup test are shown in Fig. 18. Owing to the non-uniform distribution of caves and fractures within the reservoir, as well as the impact of the underlying aquifer, a substantial water cut near the wellbore is observed. This non-uniform distribution leads to uneven pressure and saturation levels within the reservoir.

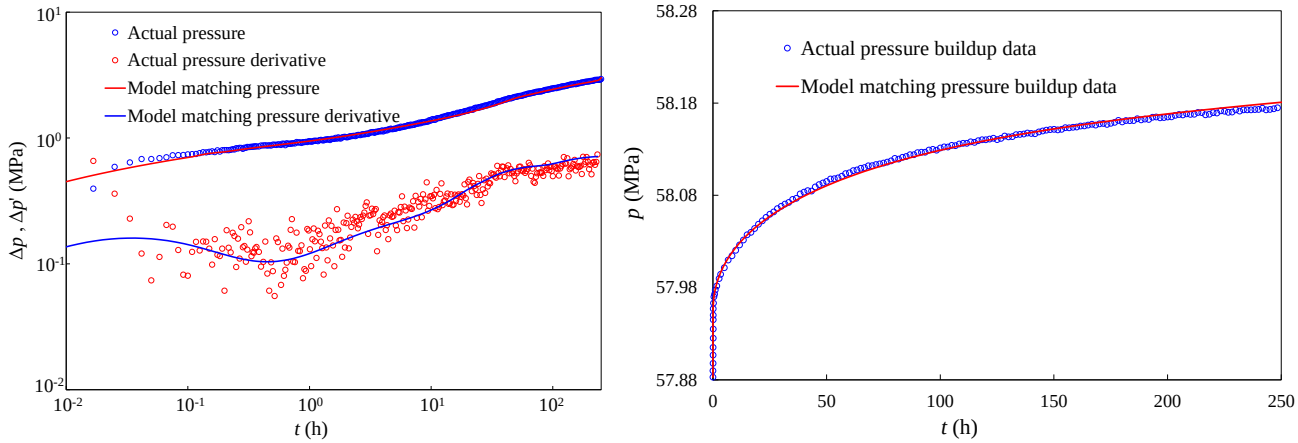

(a) Log-log plot (b) Pressure history

Fig. 17. Matching curves.

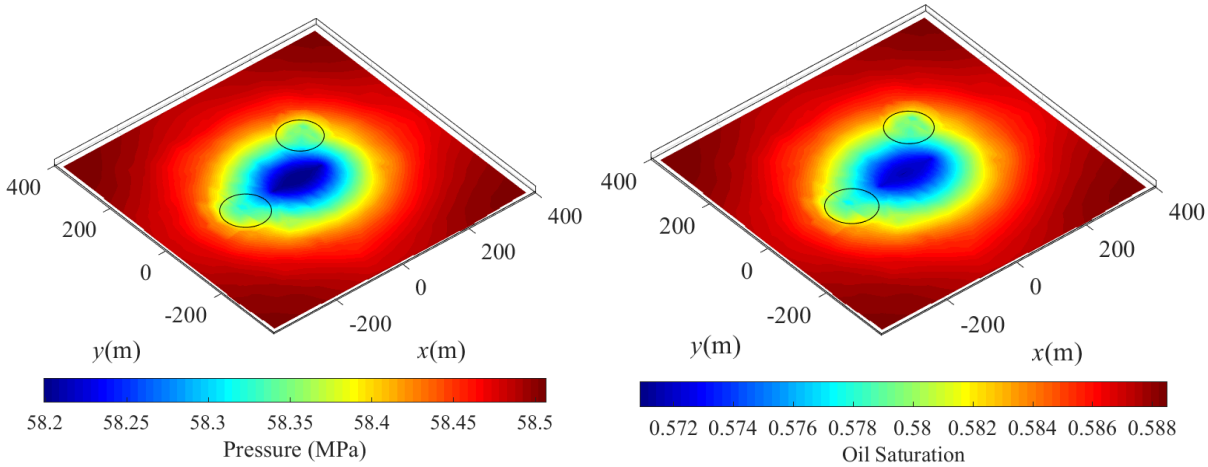

(a) Pressure field plot (b) Oil saturation field plot

Fig. 18. Physical field plot after pressure buildup test.

Table 4. Parameter interpretation result.

Parameter	Value
Initial pressure, MPa	58.71
Matrix permeability, mD	2.16
Wellbore storage coefficient, m^3/MPa	0.39
Skin	-0.2
Initial water saturation	0.4
Total volume of caves, m^3	12,360.6
Artificial fracture half length, m	40
Artificial fracture width, m	0.256
Artificial fracture height, m	15
Artificial fracture conductivity, mD·m	6,858
Drainage area, 10^4 m^2	144

Upon a comprehensive analysis of the parameter interpretations, it is discerned that the interpreted permeability k_m is 2.16 mD, indicating relatively high flow resistance within the porous rock matrix. The primary conduits for fluid flow are likely to be fractures and caves within the oil reservoir. Furthermore, the initial reservoir pressure is ascertained to be 58.71 MPa, with the maximum pressure buildup recorded during the test period reaching 58.18 MPa. This observation indicates that the well exhibits substantial production potential and can sustain stable production at a high rate for an extended duration. This outcome underscores the efficacy of the acid fracturing treatment, as reflected in the substantial artificial fracture conductivity quantified at 6,858 mD·m. The total volume of the caves V_v is determined to be 12,360.6 m^3. This result shows that the reservoir is significantly influenced by the cave interporosity flow.

4. Conclusions

This study explores the two-phase flow of oil and water within a fractured and vuggy carbonate reservoir. Randomly

generated natural fractures are integrated into the reservoir, and the fluid flow within the cavities is described using the Hagen-Poiseuille law. This enables the coupling of flow between the caves, fractures and the porous rock matrix. A mathematical model for two-phase oil-water flow in fractured carbonate reservoirs with a bottom aquifer is established. The computational domain is discretized using perpendicular bisection grids and the model is solved using the finite volume method. The pressure and pressure derivatives at different time intervals are obtained, the well test type curves are plotted, and the flow regimes are classified based on the curves.

Through a sensitivity analysis of different parameters on the well test type curves, it becomes evident that considering the presence of a bottom aquifer zone reduces the reservoir flow resistance. This reduction leads to an increase in total fluid mobility and improved fluid flow. Consequently, the well test curve exhibits a smoother trend during the interporosity flow regime. The presence of natural fractures reduces the pressure transmission consumption in the reservoir, resulting in a dip in the well test curve during the cave interporosity flow and natural fracture effect regime. The volume, quantity and location of caves primarily influence the shape of the well test curve during the cave interporosity flow regime. Larger volumes, greater quantities and a closer proximity of vuggy zones to the well extend the duration of their influence during this regime, resulting in a more pronounced ”dip” in the pressure derivative curve.

The established model is applied to interpret the pressure buildup data from well A within a fractured and vuggy carbonate reservoir, leading to the acquisition of pressure field plots and saturation field plots after the pressure buildup. The results demonstrate a strong alignment with the well test curve, affirming the suitability of the model for fractured and vuggy carbonate reservoirs. This study establishes a theoretical foundation for developing a numerical well test model for such reservoirs and holds significant importance for guiding the interpretation of pressure transient data.

Acknowledgements

The authors gratefully acknowledge the support of the National Science and Technology Major Project of SINOPEC (No. 2016ZX05014-004-001) and the Natural Science Foundation of Heilongjiang Province (No. LH2022E023) in preparing this paper.

Conflict of interest

The authors declare no competing interest.

References

Cayeux, E., Skadsem, H., Daireaux, B., et al. Challenges and solutions to the correct interpretation of drilling friction tests. Paper SPE/IADC-184657 Presented at SPE/IADC Drilling Conference and Exhibition, The Hague, The Netherlands, 14-16 March, 2017.

Chen, P., Wang, X., Liu, H., et al. A pressure-transient model for a fractured-vuggy carbonate reservoir with large-scale cave. Geosystem Engineering, 2015, 19(2): 69-76.

Corbett, P., Geiger, S., Borges, L., et al. The third porosity system: Understanding the role of hidden pore systems in well-test interpretation in carbonates. Petroleum Geoscience, 2012, 18(1): 73-81.

Dong, Y., Tian, W., Li, P., et al. Numerical investigation of complex hydraulic fracture network in naturally fractured reservoirs based on the XFEM. Journal of Natural Gas Science and Engineering, 2021, 96: 104272.

Du, X., Li, Q., Lu, Z., et al. Pressure transient analysis for multi-vug composite fractured vuggy carbonate reservoirs. Journal of Petroleum Science and Engineering, 2020, 193: 107389.

Guo, J., Nie, R., Jia, Y. Dual permeability flow behavior for modeling horizontal well production in fractured-vuggy carbonate reservoirs. Journal of Hydrology, 2012, 464: 281-293.

Huang, W., Cui, Y., Xu, F., et al. An innovative approach to permeability estimation of the fractured-vuggy carbonate reservoirs based on 2D images. Journal of Petroleum Science and Engineering, 2021, 199: 108293.

Jia, Y., Fan, X., Nie, R., et al. Flow modeling of well test analysis for porous-vuggy carbonate reservoirs. Transport in Porous Media, 2013, 97: 253-279.

Jiao, F. Practice and knowledge of volumetric development of deep fractured-vuggy carbonate reservoirs in Tarim Basin, NW China. Petroleum Exploration and Development, 2019, 46(3): 576-582.

Kamal, M., Morsy, S., Suleen, F., et al. Determination of in-situ reservoir absolute permeability under multiphase-flow conditions using transient well testing. SPE Reservoir Evaluation and Engineering, 2019, 22(1): 336-350.

Kang, Z., Wu, Y., Li, J., et al. Modeling multiphase flow in naturally fractured vuggy petroleum reservoirs. Paper SPE 102356 Presented at SPE Annual Technical Conference and Exhibition, San Antonio, Texas, 24-27 September, 2006.

Kolin, S., Kurevija, T., Grebenar, D. Pressure build-up test analysis of the reservoir system with the multiphase flow. Rudarsko-geološko-naftni zbornik, 2018, 33(3): 75-84.

Li, Y., Wang, D. Development strategy optimization of gas injection huff and puff for fractured-caved carbonate reservoirs. Paper SPE 182746 Presented at SPE Kingdom of Saudi Arabia Annual Technical Symposium and Exhibition, Dammam, Saudi Arabia, 25-28 April, 2016.

Li, Y., Wang, Q., Li, B., et al. Dynamic characterization of different reservoir types for a fractured caved carbonate reservoir. Paper SPE 188113 Presented at SPE Kingdom of Saudi Arabia Annual Technical Symposium and Exhibition, Dammam, Saudi Arabia, 24-27 April, 2017.

Lin, J., He, H., Wang, Y. A well test analysis model of generalized tube flow and seepage coupling. Petroleum Exploration and Development, 2021, 48(4): 923-934.

Liu, H. Semi-analytical solution for bottomhole pressure transient analysis of a hydraulically fractured horizontal well

in a fracture-cavity reservoir. Scientific Reports, 2022, 12: 22095.

Liu, B., Jin, Y., Chen, M. Influence of vugs in fractured-vuggy carbonate reservoirs on hydraulic fracture propagation based on laboratory experiments. Journal of Structural Geology, 2019, 124: 143-150.

Liu, S., Liu, Z., Zhang, Z., et al. Numerical study on hydraulic fracture-cavity interaction in fractured-vuggy carbonate reservoir. Journal of Petroleum Science and Engineering, 2022, 213: 110426.

Liu, J., Liu, Z., Zou, N., et al. A well test model study of multi fracture-vug combination for fractured vuggy carbonate reservoirs. Paper ID 444 Presented at International Conference on Applied Energy, Bangkok/Virtual, 1-10 December, 2020.

Lu, X., Wang, Y., Yang, D., et al. Characterization of paleokarst reservoir and faulted karst reservoir in Tahe Oilfield, Tarim Basin, China. Advances in Geo-Energy Research, 2020, 4(3): 339-348.

Nie, R. S., Jia, Y. L., Yu, J., et al. The transient well test analysis of fractured-vuggy triple-porosity reservoir with the quadratic pressure gradient term. Paper SPE 120927 Presented at 2009 SPE Latin American and Caribbean Petroleum Engineering Conference, Cartagena, Colombia, 31 May-3 June, 2009.

Popov, P., Bi, L., Efendiev, Y., et al. Multiphysics and multiscale methods for modeling fluid flow through naturally fractured vuggy car-bonate reservoirs. Paper SPE 105378 Presented at 15th SPE Middle East Oil & Gas Show and Conference held in Bahrain International Exhibition Centre, Kingdom of Bahrain, 11-14 March, 2007.

Spence, S. Keeping the promises-A management framework for delivering ESIA commitments during pipeline construction. Paper SPE 86732 Presented at Seventh SPE International Conference on Health, Safety, and Environment in Oil and Gas Exploration and Production held in Calgary, Alberta, Canada, 29-31 March, 2004.

Sun, H., Ouyang, W., Zhu, S., et al. A new numerical well test method of multi-scale discrete fractured tight sandstone gas reservoirs and its application in the Kelasu Gas Field of the Tarim Basin. Natural Gas Industry B, 2023, 10(2): 103-113.

Sun, J., Schechter, D. Optimization-based unstructured meshing algorithms for simulation of hydraulically and naturally fractured reservoirs with variable distribution of fracture aperture, spacing, length, and strike. SPE Reservoir Evaluation & Engineering, 2015, 18(4): 463-480.

Tang, B., Ren, K., Lu, H., et al. Study on residual oil distribution law during the depletion production and water flooding stages in the fault-karst carbonate reservoirs. Processes, 2023, 11: 2147.

Tian, F., Luo, X., Zhang, W. Integrated geological-geophysical characterizations of deeply buried fractured-vuggy carbonate reservoirs in Ordovician strata, Tarim Basin. Marine and Petroleum Geology, 2019, 99: 292-309.

Wang, Y., Yu, H., Zhang, J., et al. Transient pressure analysis of polymer flooding fractured wells with oil-water two-phase flow. Petroleum Exploration and Development, 2023, 50(1): 175-182.

Xie, F., Zhang, C., Liu, R., et al. Production prediction for fracture-vug carbonate reservoirs using electric imaging logging data. Petroleum Exploration and Development, 2018, 45(2): 369-376.

Xing, C., Yin, H., Liu, K., et al. Well test analysis for fractured and vuggy carbonate reservoirs of well drilling in large scale cave. Energies, 2018, 11(1): 80.

Yang, B., He, J., Lyu, D., et al. Production optimization for water flooding in fractured-vuggy carbonate reservoir-From laboratory physical model to reservoir operation. Journal of Petroleum Science and Engineering, 2020, 184: 106520.

Zhang, Q., Yan, Z., Fan, X., et al. Field monitoring and identification method for overflow of fractured-vuggy carbonate reservoir. Energies, 2023, 16(5): 2399.

Zhang, T., Zeng, X., Guo, J., et al. Numerical simulation on oil-water-particle flows in complex fractures of fractured-vuggy carbonate reservoirs. Journal of Petroleum Science and Engineering, 2022, 208: 109413.